Self-Cleaning Organic/Inorganic Photo-Sensors

Athanasios Milionis,*[†, ‡] Roberto Giannuzzi,[‡] Ilker S. Bayer,[†] Evie L. Papadopoulou,*[†] Roberta Ruffilli,[§] Michele Manca,[‡] and Athanassia Athanasiou*[†]

[†]Nanophysics, Istituto Italiano di Tecnologia (IIT), Via Morego 30, 16163 Genova, Italy

[‡]Center for Biomolecular Nanotechnologies (CBN) @UNILE, Istituto Italiano di Tecnologia (IIT), Via Barsanti, 73010 Arnesano (LE), Lecce, Italy

[§]Nanochemistry, Istituto Italiano di Tecnologia (IIT), Via Morego 30, 16163 Genova, Italy

S *Supporting Information*
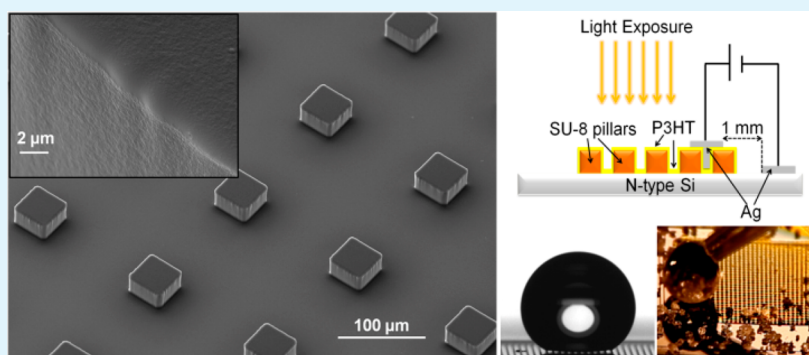
ABSTRACT: We present the fabrication of a multifunctional, hybrid organic−inorganic micropatterned device, which is capable to act as a stable photosensor and, at the same time, displaying inherent superhydrophobic self-cleaning wetting characteristics. In this framework several arrays of epoxy photoresist square micropillars have been fabricated on n-doped crystalline silicon substrates and subsequently coated with a poly(3-hexylthiophene-2,5-diyl) (P3HT) layer, giving rise to an array of organic/inorganic p−n junctions. Their photoconductivity has been measured under a solar light simulator at different illumination intensities. The current−voltage (I−V) curves show high rectifying characteristics, which are found to be directly correlated with the illumination intensity. The photoresponse occurs in extremely short times (within few tens of milliseconds range). The influence of the interpillar distance on the I−V characteristics of the sensors is also discussed. Moreover, the static and dynamic wetting properties of these organic/inorganic photosensors can be easily tuned by changing the pattern geometry. Measured static water contact angles range from 125° to 164°, as the distance between the pillars is increased from 14 to 120 μm while the contact angle hysteresis decreases from 36° down to 2°.

KEYWORDS: *self-cleaning, solar sensor, p−n heterojunction, micropillars, P3HT, SU-8*

1. INTRODUCTION

Organic/inorganic photodiodes have attracted considerable interest during the past few years; especially due to their low cost, simplicity, and their unique mechanical properties. They are considered very promising candidates for the fabrication of flexible electronic devices.[1−5] Most of such organic/inorganic hybrids are incorporated with nanoparticles or nanorods to improve their functionality. However, these nanomaterials often require demanding and expensive synthetic routes, and at the same time, controlling their dispersion and size distribution can be quite challenging. There is a wide range of possible applications of organic/inorganic nanocomposites, including photodetectors,[6] photovoltaic devices,[7] optical fibers,[8] and sensors.[9] Organic/inorganic photodiodes made of silicon in junction with various functional polymers, without the use of nanofillers and with improved efficiency of photodetection in the UV range have been recently demonstrated in the literature.[10,11] This approach can take advantage of the existing silicon-based integrated technology.

P3HT is an organic semiconductor that has been mainly used for the fabrication of transistors,[12] photovoltaic cells,[13,14] strain sensors,[15] and light emitting devices.[16] Its combination with crystalline silicon has been examined for the fabrication of solar cells. In particular, silicon nanocrystals have been incorporated in the P3HT matrix to produce nanocomposite materials that enhance the solar cell performance.[17−19] P3HT and silicon have been also used in their bulk form. The influence of nanoscale structuring for increasing the aspect ratio of their interface has been investigated with the perspective of increasing the power conversion efficiency.[20] The transport

effects on the interface between P3HT and n-Si heterojunction have also been examined.[21−24]

If hybrid organic−inorganic photosensors designed for use in ambient outdoor conditions displayed inherent self-cleaning properties,[25] their maintenance would be easier and their lifetime would be drastically prolonged due to removal of contaminants and dirt by rolling-off of water droplets impinging on their surfaces.[26−28] However, to the best of our knowledge, there are no detailed reports on the fabrication and characterization of patterned P3HT/crystalline silicon junctions that function as self-cleaning photodiodes.

In the present study, we used a standard photolithographic method to fabricate a periodic array of micropillars made of a photoresist material on silicon. Different microstructures were fabricated by tuning the fill factor of the pillars. Subsequently, P3HT was solution deposited on the patterned area to generate a p−n junction at the interface with silicon. The degree of hydrophobicity and water adhesion were investigated, and the water apparent contact angle and contact angle hysteresis were found to be dependent on the interpillar distance, d_{int}. A self-cleaning behavior was observed for relatively large d_{int} values. The resulting structures were found to exhibit excellent geometry dependent photoresponsive characteristics.

2. EXPERIMENTAL SECTION

2.1. Materials. N-type silicon wafers doped with phosphor (Jocam, Italy) and SU-8 3050 photoresist (Microchem, U.S.A.) were used as received. P3HT and all solvents used were purchased from Sigma-Aldrich. 0.5 wt % P3HT was dissolved in chloroform and left under stirring for 1 h until a reddish, homogeneous solution was obtained.

2.2. Fabrication of SU-8/P3HT Micropillars. According to the manufacturer, 1 mL of SU-8 3050 is needed to be dispensed for a 25 mm diameter substrate such as a standard silicon wafer. Accordingly, wafers were spin-coated based on the manufacturer recommendation. Spin-coating steps were as follows: (1) at 500 rpm for 10 s with acceleration 100 rpm/s and (2) at 4000 rpm for 30 s with acceleration 300 rpm/s. Next, the samples were soft-baked at 100 °C for 20 min on a hot plate. The thickness of the film obtained was 33 μm. Sodalime masks of square-shaped patterns (42 μm side) (Deltamask Netherlands) with various intersquare distances were used for the exposure of the spin-coated samples. Patterning was performed by exposing the spin-coated material to UV radiation with a Karl-Suss MA6 mask-aligner in hard contact mode with an i-line mercury lamp. An exposure dose of 323 mJ was used to fully polymerize the 33 μm thick SU-8 layer. Exposure was followed by postbake on a hot plate at 65 °C for 1 min and at 95 °C for 5 min. The samples were then allowed to cool and washed for 4 min with SU-8 developer, followed by rinsing with 2-propanol. Square micropillars of H = 33 μm height and α = 42 μm width were obtained after the fabrication process. The interpillar distance, d_{int}, was varied from 14 μm up to 120 μm. Figure 1 depicts a diagram with the geometrical characteristics of the micropillar arrays. Subsequently, 10 μL of the P3HT solution was drop-casted onto the micropillars and was left in a chemical hood until the solvent was completely evaporated. The P3HT conformed to the microstructured surfaces, creating a coating layer of approximately 750 nm thickness. Note that, after developing the samples with the SU-8 developer, silicon wafer surfaces were exposed at interpillar regions.

2.3. Wetting Measurements. Apparent contact angle (APCA) and contact angle hysteresis (CAH) measurements were carried out using a KSVCAM200 contact angle goniometer (Kruss, Germany). 8 μL drops of deionized water were placed on at least 10 samples prepared with the same procedure. The advancing and receding contact angles were measured by dispensing and retracting water until a motion of the contact line on the surface was observed. The standard deviation of the measurements was ±3°. All measurements were performed in ambient conditions.

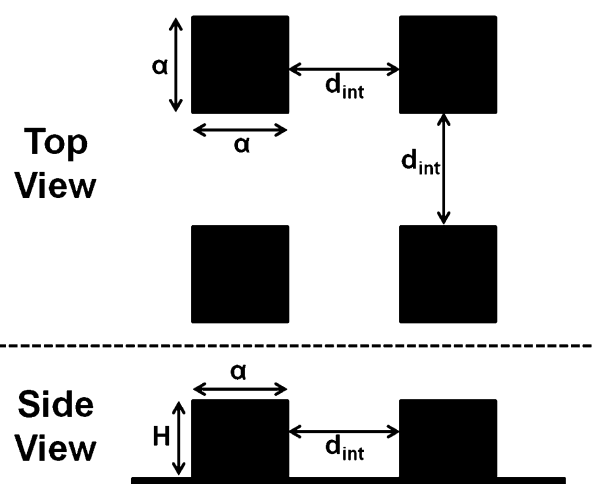**Figure 1.** Top and side view diagram of the geometrical parameters of the square micropillars. α = 42 μm (square side), d_{int} is the interpillar distance (ranging from 14 to 120 μm), and H = 33 μm is the pillar height.

2.4. Surface Characterization. The morphology of the patterned surfaces was characterized by scanning electron microscopy (SEM, JEOL JSM-6490LA). Atomic force microscopy (AFM) measurements were performed with a Park Systems XE-100 in noncontact mode. The optical images were acquired with a Canon EOS 5D Mark II camera equipped with a Canon EF 100 mm f/2.8 L IS USM Macro objective lens.

2.5. Transport and Light Response Measurements. The electrical characteristics of the samples were measured using an Autolab 302N potentiostat interfaced with a Karl Suss RA150 Probe Station. Ohmic contacts were prepared with silver paste, at 1 mm distance. The current−voltage curves were measured by scanning potential applied on the devices from −5 to 5 V at a scan rate of 50 mV/s. The measurements were performed in dark and under illumination with power densities ranging from 0 to 110 mW/cm^2. The light source was a solar light simulator (Cool White (5650K), Luxeon, U.S.A.). Photocurrent transients were recorded by using an exciting pulse that was generated by the light source.

3. RESULTS AND DISCUSSION

Figure 2 depicts SEM images of the SU-8 micropillars coated with the P3HT. The initial geometry and the structure of the SU-8 micropillars are maintained since P3HT forms a conformal coating on them. However, a more detailed surface analysis by AFM measurements on the same surfaces revealed the existence of nanoscale roughness, as indicated by the arrows in Figure 2. The root-mean-square roughness calculated by the AFM images was 12 nm for the P3HT casted on silicon and 14 nm for the P3HT casted on the SU-8 pillars. Therefore, in terms of topographical characteristics, a dual-scale roughness is unveiled due to the SU-8 micropatterns and the inherent nanoroughness of the solution-cast P3HT. The combination of at least two scales of roughness is required in self-cleaning superhydrophobic surfaces,[29] since the addition of a second roughness scale on hydrophobic microrough surfaces is usually responsible for the increase of the APCA and the elimination of CAH.[30−33] In our system, the experimentally measured APCA ranges from 125° to 164° for d_{int} 14 to 120 μm, respectively, as shown in Figure 3a. Evidently, the structures become superhydrophobic for d_{int} greater than 63 μm. The effect of the surface roughness on the wettability has been modeled theoretically by two standard approaches, namely the Wenzel[34] and the Cassie−Baxter.[35] The application of these models to
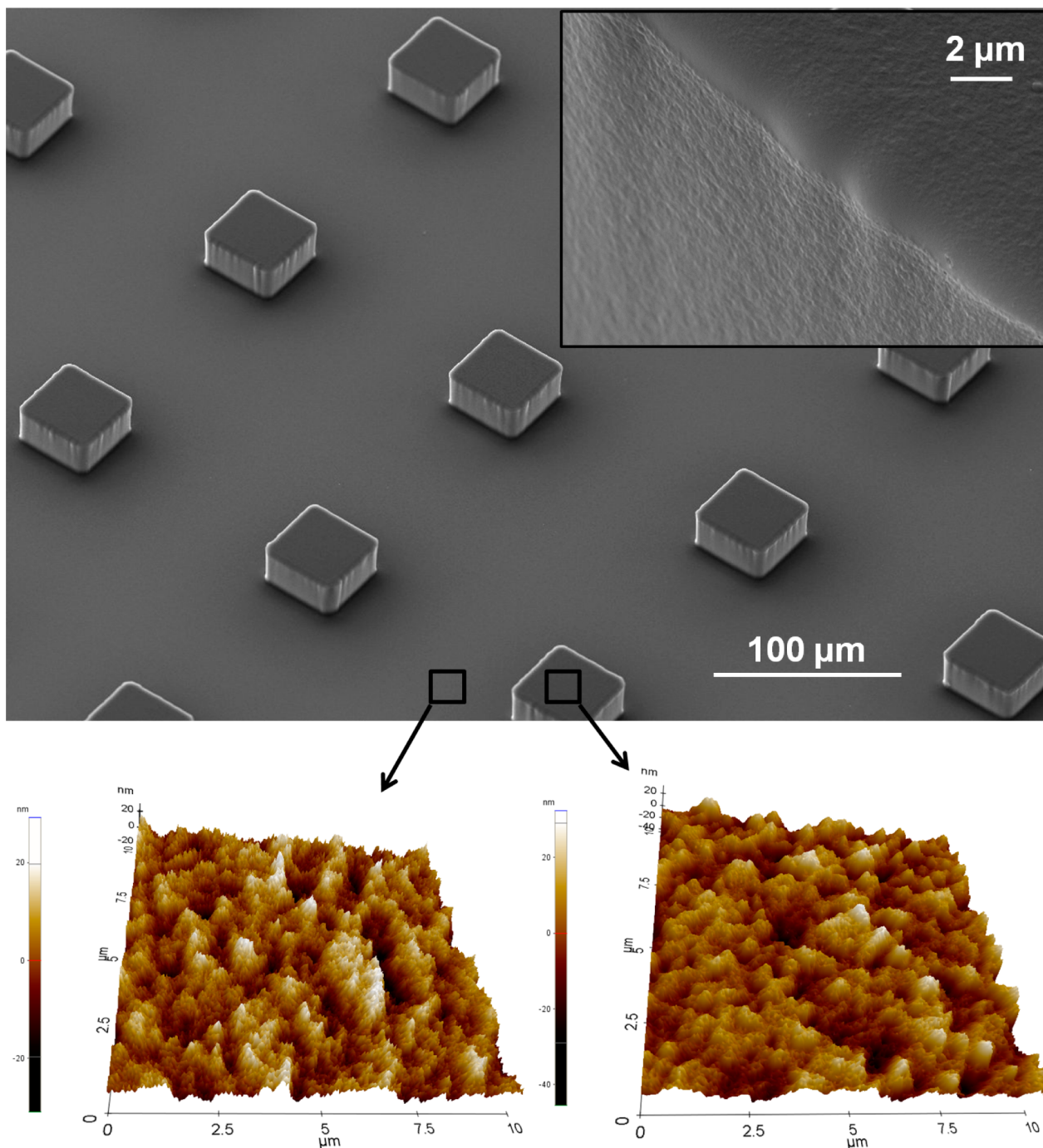
Figure 2. Top: Low-magnification SEM image of the SU-8 micropillars on silicon, with d_{int} = 77 μm, coated with P3HT. Inset: High-magnification SEM image of the topography of the P3HT coating. Bottom: AFM images of the P3HT coating on silicon and on top of an SU-8 pillar. The arrows indicate the corresponding areas that the AFM scanning was performed.

the square-type pillar-geometries[36] used in this study is used to interpret the aforementioned results.

According to the Wenzel model, a water droplet residing on a rough surface penetrates in the recessed regions, tending to increase the interfacial contact area with the solid, until a complete wetting condition is eventually maintained. The APCA, θ_w, is given by

$$\cos(\theta_w) = r \cos(\theta_Y) \qquad (1)$$

where r is the actual over the projected surface area of the substrate and θ_Y is the intrinsic contact angle on a flat surface of

the same nature as the rough, namely the Young's contact angle. The contact angle of the P3HT film deposited on a flat substrate was measured to be 104°, and this value was used for the theoretical calculations.

In contrast, the Cassie–Baxter model assumes that the water does not penetrate into the rough features. As a result, air gets trapped into the recessed regions under the liquid, which now is sitting in a composite surface, made of solid and air. The contact angle is now given by

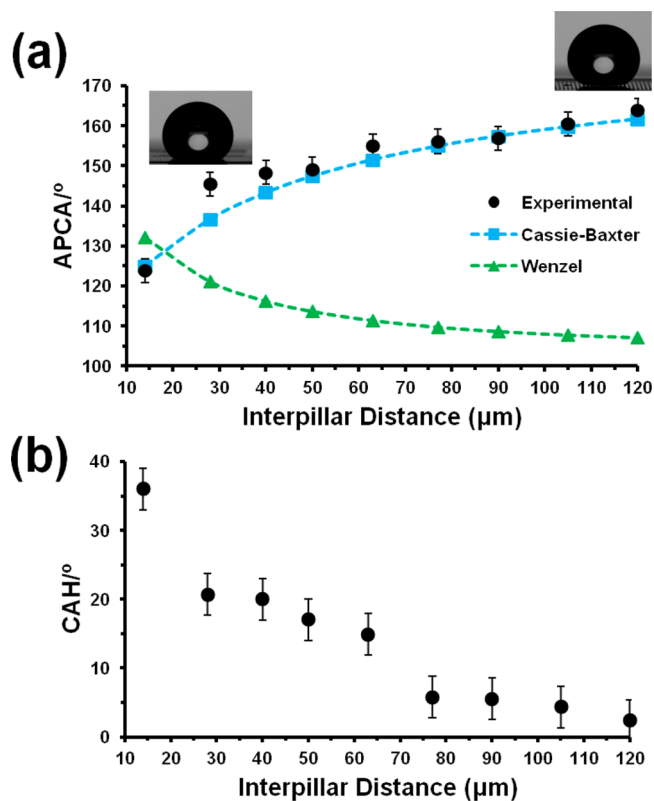$$\cos(\theta_{CB}) = f_{SL}[\cos(\theta_Y) + 1] - 1 \qquad (2)$$

Figure 3. (a) Static (APCA) and (b) dynamic (CAH) wetting characteristics of the P3HT coated patterns for different d_{int}.

where θ_{CB} is the APCA of the rough surface and f_{SL} is the fractional geometrical area of the solid−liquid interface under the drop.

For the pillar geometries fabricated in this work, r and f_{SL} can be written as[36]

$$r = 1 + \frac{4f_{SL}}{(a/H)} \qquad (3)$$

$$f_{SL} = \frac{1}{(b/a + 1)^2} \qquad (4)$$

where a is the side of the square-shaped pillars ($a = 42\ \mu$m), H is the height of the pillars ($H = 33\ \mu$m), and b is the d_{int} (Figure 1). In Figure 3a, the contact angle values calculated from the above-mentioned theoretical models, using eqs 1−4, are plotted against the d_{int} of different structures. The experimental APCA values are also shown on the same diagram. It is immediately seen that the theoretical values from the Cassie−Baxter model are in good agreement with the experimental ones. It can thus be concluded that the nonwetting characteristics of the fabricated samples follow the classical Cassie−Baxter model.

The receding and advancing angles were measured in order to estimate the contact angle hysteresis (CAH), which is defined as their difference. In Figure 3b, the CAH is plotted versus the interpillar distance, and it can be seen that the CAH decreases with increasing d_{int}. Most importantly, structures with interpillar distances higher than 77 μm have an APCA larger than 156° and CAH less than 6°, which renders them self-cleaning.

Apart from their self-cleaning characteristics, these devices were also found to show good electrical response when subjected to solar light, due to the diode-like behavior of the

P3HT/silicon junctions at the interpillar spacing. Figure 4a depicts the typical $I-V$ behavior of the micropatterned array for
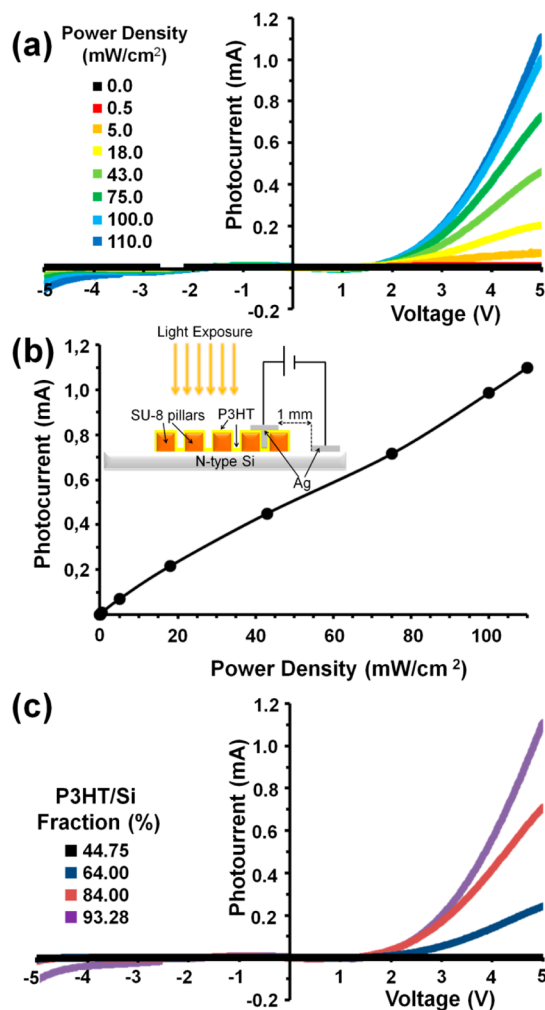

Figure 4. (a) $I-V$ characteristics of the self-cleaning patterns with d_{int} 120 μm, for different power densities. (b) Measured photocurrent for 5 V applied bias under different power densities. Inset: A sketch illustrating the configuration of the experimental setup is presented on the left part of the figure. (c) $I-V$ characteristics for different P3HT/Si fractions under constant power density (110 mW/cm²).

d_{int} = 120 μm under different illumination intensities, using a solar light simulator as a light source. The measurements were performed both in dark and in light (under different illumination intensities, ranging from 0 to 110 mW/cm²). It can be observed that the illumination with different light intensities attributes rectifying characteristics to the patterned surfaces, indicating the formation of a diode-like structure.

One important parameter when characterizing a diode is the rectification ratio (RR), defined as the ratio of the forward current divided by the reverse current at a specific bias. For high quality photodiodes, high RR values are essential. The rectification ratios (RRs) for all illumination powers shown in Figure 4a were calculated above the threshold voltage and are listed in Table 1. The threshold voltage is the voltage for which the forward current exhibits a rapid increase, resulting in the asymmetry in the I−V curves. The highest RR was 186 for 5 mW/cm² and 3 V applied bias, a very high value compared with other published RR values for hybrid systems.[2,37]

7142

dx.doi.org/10.1021/am401476k | ACS Appl. Mater. Interfaces 2013, 5, 7139−7145

Table 1. Rectification Ratio (RR) of the Pattern with d_{int} = 120 μm under Different Power Densities

power density (mW/cm^2)	RR at 1 V	RR at 2 V	RR at 3 V	RR at 4 V	RR at 5 V
0.07	5	50	21	14	16
0.50	11	55	99	59	51
5.00	13	65	186	153	152
18.00	11	36	70	83	75
43.00	9	18	35	47	53
75.00	6	12	24	30	33
100.00	4	10	18	21	23
110.00	6	8	10	12	13

Furthermore, the resultant photocurrent shows a linear dependence on the illumination intensity, for illumination intensities up to 110 mW/cm^2, as shown in Figure 4b. The detection limit was approximately 0.07 mW/cm^2. When the superhydrophobic structure is under solar illumination, photons are absorbed by the P3HT layers and result in the generation of excitons (electron–hole pairs). A certain portion of these excitons reach the P3HT/Si interface and dissociate into charge carriers (i.e., electrons and holes) because the energy decrease of the single carriers is larger than the binding energy of the excitons. These free carriers hence induce the measured photocurrent.[12,22,23,38]

The $I−V$ characteristics were measured for samples with different interpillar distances or in other words, different P3HT/Si fraction, under 110 mW/cm^2 illumination power, and they are shown in Figure 4c. It can be seen that all the structures effectively respond to the light exposure and give rise to a photocurrent with rectifying properties. The photocurrent increases 5×10^4% when the P3HT/Si fraction increases from 44.75% to 93.28% or otherwise when the interpillar distance increases from 14 to 120 μm. This is explained having in mind that only the regions in between the SU-8 pillars, where the P3HT is in direct contact with the Si substrate, are responsible for the photoconductivity. As a result, for increasing distance between the SU-8 pillars, the photocurrent produced under white light illumination also increases. Considering, thus, the aforementioned results, in conjunction with the wetting properties of the structures, we can conclude that the structures with optimized multifunctionality are the ones with the largest d_{int}, since they demonstrate the best nonwetting characteristics and the best diode properties.

These multifunctional structures of d_{int} = 120 μm were also tested under pulsed light/dark conditions in order to evaluate their photoresponse. The light source was switched on and off at definite time intervals, under a constant applied bias of 5 V while the sample was illuminated with a 100 mW/cm^2 power density. When the light source was switched on, the photocurrent rapidly increased, and when switched-off, a rapid decrease of the current to its dark value was observed.
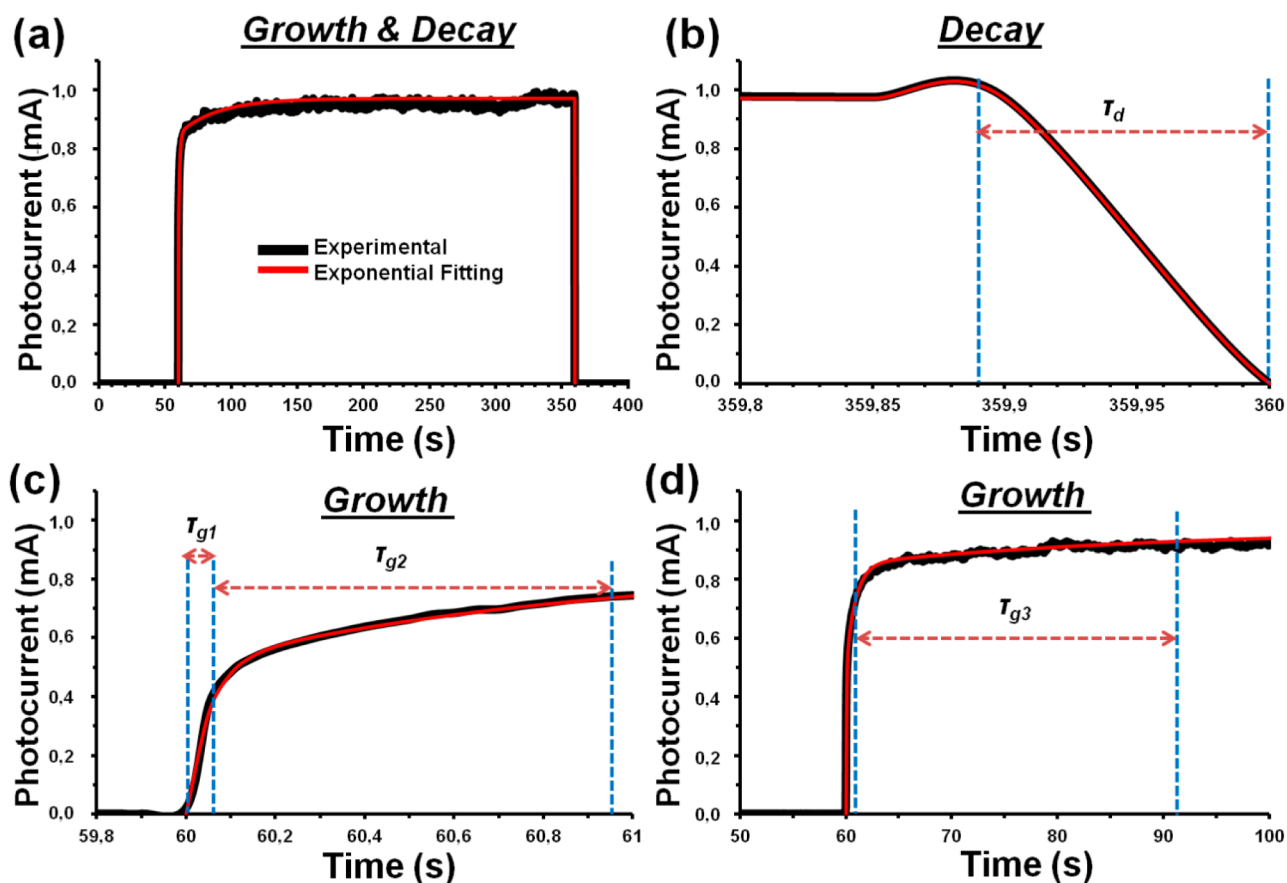

Figure 5. Graphs showing the growth and decay of the photocurrent for the pattern with d_{int} = 120 μm. (a) Single pulse with 100 mW/cm^2 power density. The black line represents the experimental photocurrent values obtained against the time evolution, while the red line is the exponential fitting. (b) Decay of the pulse after turning off the LED. (c) The first two fast parts of the triexponential growth behavior of the photocurrent after the sample is being illuminated. (d) The third (slower) part of the triexponential growth of the photocurrent.

As shown in Figure 5, the growth and decay times of the photocurrent are very short. The growth time shows two rapid components followed by a slower one. In order to calculate the time constants, the data were fitted with a triexponential function as follows:

$$I_g(t) = I_0 + A_1(1 - e^{-t/\tau_{g_1}}) + A_2(1 - e^{-t/\tau_{g_2}})$$
$$+ A_3(1 - e^{-t/\tau_{g_3}}) \quad (5)$$

where τ_{g_1}, τ_{g_2}, and τ_{g_3} are the three time constants, I_0 is the dark current, and A_1, A_2, and A_3 are positive constants. The calculated time constants, then, are $\tau_{g_1} = 50$ ms, $\tau_{g_2} = 900$ ms, and $\tau_{g_3} = 30$ s. The decay time was found to have only a rapid component following an exponential decay function:

$$I_d(t) = I_0 + A_4\, e^{t/\tau d} \quad (6)$$

where I_0 is the dark current and A_4 is a positive constant. The estimated time constant is $\tau_d = 11$ ms. The recovery time is much shorter than the ones reported in other studies on sensors with ultrafast recovery times exhibiting biexponential decay behavior with both exponentials having greater decay time constants than the one found in this work.[39,40] The on/off current ratio or photosensitivity of the patterned surfaces, defined as the ratio of the photocurrent to the dark conductivity was measured to be approximately 3.5×10^3 for 5 V applied bias and 100 mW/cm^2 power density, indicating an excellent response from the structures. Furthermore, an aging test of 100 repeated cycles was performed, in order to test the stability of the system. The light pulses used were of 200 ms duration, and they were applied periodically (every 5 s), as shown in Figure 6. It can be seen that the photocurrent produced is stable and the fluctuation is less than 25% in 10 min.
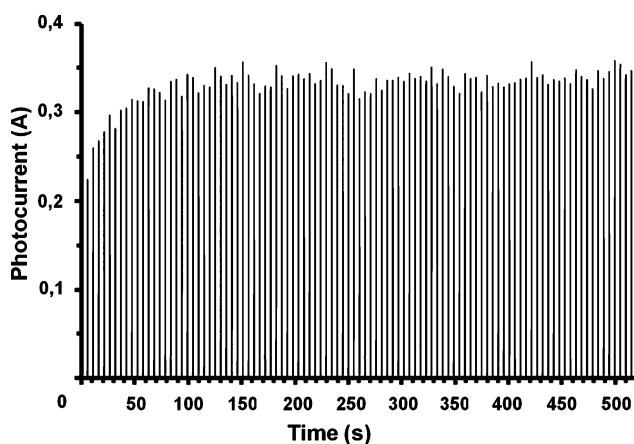

Figure 6. Durability test after 100 cycles of 0.2 s pulses of 100 mW/cm^2 power density on the pattern with $d_{int} = 120$ μm.

Finally, the self-cleaning properties of the optimal multifunctional patterned structures with $d_{int} = 120$ μm were demonstrated by performing a simple dust removal experiment using moving droplets as shown in Figure 7. Parts a and b of Figure 7 depict a patterned surface clean and covered with KCl powder, respectively. Subsequently, the powder is successfully removed by allowing a water droplet to move over the surface of the samples, as shown in Figure 7c and d. The water droplet picks up the powder while moving and removes it from the photosensitive surface (see Videos 1−3 in the Supporting Information). Thus, the photoactive surface retains its
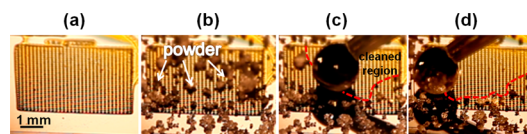

Figure 7. Dust removal experiment on the pattern with $d_{int} = 120$ μm. (a) Photograph of the as fabricated self-cleaning pattern. (b) Photograph of the randomly deposited KCl powder on the surface to simulate contamination. (c and d) Photographs of a water droplet attached to the tip of a pipet moving over the surface picking up the powder on its way.

efficiency in detecting the solar light, which otherwise could be reduced by scattering effects due to the presence of such dust or dirt particles in the optical path between the light source and the photosensitive material. Moreover, the patterns can easily repel even impinging water jets without being saturated by the high water pressure induced (see Video 4 in the Supporting Information). Hence, the developed patterned p−n heterojunctions can be used in conjunction with other devices that need to be water resistant.

4. CONCLUSIONS

In summary, we have fabricated fast-photoresponsive 3D organic/inorganic p−n junctions, made of P3HT-coated SU-8 periodic micropillars on silicon. The structures exhibit self-cleaning properties. Both the photosensitivity and the wetting properties can be controlled by tuning the geometrical features. The photoresponse of the sensors illuminated with different power densities has been examined. These sensors exhibit excellent robustness and stability after several hundred of cycles of light switching. As a result, they can be considered as suitable candidates for a wide range of photodetection applications in which hydrorepellency is mostly required.

■ ASSOCIATED CONTENT

Ⓢ Supporting Information
Videos demonstrating the self-cleaning properties of the fabricated photosensors. Video 1. A droplet, not sticking to the patterned surface ($d_{int} = 120$ μm) due to the very low CAH. Video 2. KCl powder placed on the same patterned surface. Video 3. A droplet is moving and on its way removes the powder. Video 4. A water jet hits the patterned surface and it is repelled. Its approximate velocity when it comes in contact with the pattern is 1 m/s. The surface remains undamaged. This information is available free of charge via the Internet at http://pubs.acs.org/.

■ AUTHOR INFORMATION

Corresponding Author
*E-mail: athanasios.milionis@iit.it, paraskevi.papadopoulou@iit.it, athanassia.athanassiou@iit.it.

Author Contributions
The manuscript was written through contributions of all authors. All authors have given approval to the final version of the manuscript.

Notes
The authors declare no competing financial interest.

■ ABBREVIATIONS

P3HT, poly(3-hexylthiophene-2,5-diyl); APCA, apparent contact angle; CAH, contact angle hysteresis; d_{int}, interpillar

distance; SEM, scanning electron microscopy; AFM, atomic force microscopy; RR, rectification ratio

■ REFERENCES

(1) Guo, Y.; Tang, Q.; Liu, H.; Zhang, Y.; Li, Y.; Hu, W.; Wang, S.; Zhu, D. *J. Am. Chem. Soc.* **2008**, *130*, 9198−9199.

(2) Karan, S.; Mallik, B. *Nanotechnology* **2008**, *19*, 495202.

(3) Yuan, Z.; Yu, J.; Wang, N.; Jiang, Y. *Curr. Appl. Phys.* **2012**, *12*, 1278−1282.

(4) Pradhan, B.; Sharma, A. K.; Ray, A. K. *J. Phys. D.: Appl. Phys.* **2009**, *16*, 165308.

(5) Ma, W.; Yu, J.; Yuan, Z.; Jiang, Y. *Integr. Ferroelectr.* **2011**, *128*, 149−154.

(6) Wang, L.; Zhao, D.; Su, Z.; Fang, F.; Li, B.; Zhang, Z.; Shen, D.; Wang, X. *Org. Electron.* **2010**, *11*, 1318−1322.

(7) Xue, J.; Rand, B. P.; Uchida, S.; Forrest, S. R. *Adv. Mater.* **2005**, *17*, 66−71.

(8) Molina, C.; Victoria, L.; Arenas, A. *J. Chem. Educ.* **2004**, *81*, 1333.

(9) Caramia, V.; Bayer, I. S.; Anyfantis, G. C.; Ruffilli, R.; Ayadi, F.; Martiradonna, L.; Cingolani, R.; Athanassiou, A. *Nanotechnology* **2013**, *24*, 055602.

(10) Levell, J. W.; Giardini, M. E.; Samuel, I. D. W. *Opt. Express* **2010**, *4*, 3219−3225.

(11) Cardenas, J. R.; de Vasconcelos, E. A.; de Azevedo, W. M.; da Silva, E. F.; Pepe, I.; Ferreira da Silva, A.; Santedicola Ribeiro, S.; Abreu Silva, K. *Appl. Surf. Sci.* **2008**, *255*, 688−690.

(12) Yan, F.; Li, J.; Mok, S. M. *J. Appl. Phys.* **2009**, *106*, 074501.

(13) Tao, C.; Aljada, M.; Shaw, P. E.; Lee, K. H.; Cavaye, H.; Balfour, M. N.; Borthwick, R. J.; James, M.; Burn, P.; Gentle, I. R.; Meredith, P. *Adv. Energy Mater.* **2013**, *3*, 105−112.

(14) Kim, D. H.; Lee, Y. H.; Lee, D. U.; Kim, T. W.; Kim, S.; Kim, S. W. *Opt. Express* **2012**, *10*, 10476−10483.

(15) Ryu, D.; Loh, K. J. *Smart Mater. Struct.* **2012**, *21*, 065017.

(16) Biswas, A.; Bayer, I. S.; Karulkar, P. C.; Tripathi, A.; Avasthi, D. K. *J. Appl. Phys.* **2007**, *102*, 083543.

(17) Herrmann, D.; Niesar, S.; Scharsich, C.; Kohler, A.; Strutzmann, M.; Riedle, E. *J. Am. Chem. Soc.* **2011**, *133*, 18220−18233.

(18) Liu, C. Y.; Holman, Z. C.; Kortshagen, U. W. *Nano Lett.* **2009**, *9*, 449−452.

(19) Svrcek, V.; Turkevych, I.; Kondo, M. *Nanoscale Res. Lett.* **2009**, *4*, 1389−1394.

(20) Alet, P. J.; Palacin, S.; Cabarrocas, P. R. I.; Kalache, B.; Firon, M.; de Bettignies, R. *Eur. J. Appl. Phys.* **2006**, 231−234.

(21) Nolasco, J. C.; Cabre, R.; Ferre-Borrull, J.; Marsal, L. F.; Estrada, M.; Pallares, J. *J. Appl. Phys.* **2010**, *107*, 044505.

(22) Avasthi, S.; Sturm, J. C. In *Photovoltaic Specialists Conference (PVSC), 37th IEEE*, Seattle, WA, June 19−24, 2011.

(23) Sang, Y.; Liu, A.; Liu, W.; Kang, D. *Vacuum* **2012**, *86*, 2158−2161.

(24) Sang, Y.; Liu, W.; Qiao, F.; Kang, D.; Liu, A. *Vacuum* **2013**, *93*, 28−30.

(25) Yuan, L.; Dai, J.; Fan, X.; Song, T.; Tao, Y. T.; Wang, K.; Xu, Z.; Zhang, J.; Bai, X.; Lu, P.; Chen, J.; Zhou, J.; Wang, Z. L. *ACS Nano* **2011**, *5*, 4007−4013.

(26) Artus, G. R. J.; Jung, S.; Zimmermann, J.; Gautschi, H. P.; Marquardt, K.; Seeger, S. *Adv. Mater.* **2006**, *18*, 2758−2762.

(27) Prevo, B. G.; Hon, E. W.; Velev, O. D. *J. Mater. Chem.* **2007**, *17*, 791−799.

(28) Min, W. L.; Jiang, B.; Jiang, P. *Adv. Mater.* **2008**, *20*, 3914−3918.

(29) Gao, L.; McCarthy, T. J. *Langmuir* **2006**, *22*, 2966−2967.

(30) Milionis, A.; Martiradonna, L.; Anyfantis, G. C.; Cozzoli, P. D.; Bayer, I. S.; Fragouli, D.; Athanassiou, A. *Colloid Polym. Sci.* **2013**, *291*, 401−407.

(31) Bayer, I. S.; Brandi, F.; Cingolani, R.; Athanassiou, A. *Colloid Polym. Sci.* **2013**, *291*, 367−373.

(32) Papadopoulou, E. L.; Berberoglou, M.; Zorba, V.; Manousaki, A.; Pagkozidis, A.; Stratakis, E.; Fotakis, C. *J. Phys. Chem. C* **2009**, *113*, 2891−2895.

(33) Bayer, I. S.; Fragouli, D.; Attanasio, A.; Sorce, B.; Bertoni, G.; Brescia, R.; Di Corato, R.; Pellegrino, T.; Kalyva, M.; Sabella, S.; Pompa, P. P.; Cingolani, R.; Athanassiou, A. *ACS Appl. Mater. Interfaces* **2011**, *3*, 4024−4031.

(34) Wenzel, R. N. *Ind. Eng. Chem.* **1936**, *28*, 988−994.

(35) Cassie, A. B. D.; Baxter, S. *Faraday Soc.* **1944**, *40*, 546−551.

(36) Zhu, L.; Feng, Y.; Ye, X.; Zhou, Z. *Sens. Actuators A* **2006**, *130*, 595−600.

(37) Novotny, C. J.; Yu, E. T.; Yu, P. K. L. *Nano Lett.* **2008**, *8*, 775−779.

(38) Yuan, Z.; Yu, J.; Ma, W.; Jiang, Y. *Appl. Phys. A: Mater. Sci. Process.* **2012**, *106*, 511−515.

(39) Zhang, X.; Han, X.; Su, J.; Zhang, Q.; Gao, Y. *Appl. Phys. A: Mater. Sci. Process.* **2012**, *107*, 255−260.

(40) Cheng, G.; Wu, X.; Liu, B.; Li, B.; Zhang, Z.; Du, Z. *Appl. Phys. Lett.* **2011**, *99*, 203105.

7145

dx.doi.org/10.1021/am401476k | *ACS Appl. Mater. Interfaces* 2013, 5, 7139−7145